Biomaterials Science

ROYAL SOCIETY OF CHEMISTRY

PAPER

View Article Online
View Journal | View Issue

Cite this: *Biomater. Sci.*, 2023, **11**, 949

Thermoresponsive shear-thinning hydrogel (T-STH) hemostats for minimally invasive treatment of external hemorrhages†

Marvin Mecwan, * Reihaneh Haghniaz, Alireza Hassani Najafabadi, Kalpana Mandal, Vadim Jucaud, Johnson V. John * and Ali Khademhosseini *

Hemorrhage is the leading cause of death following battlefield injuries. Although several hemostats are commercially available, they do not meet all the necessary requirements to stop bleeding in combat injuries. Here, we engineer thermoresponsive shear-thinning hydrogels (T-STH) composed of a thermoresponsive polymer, poly(*N*-isopropyl acrylamide) (p(NIPAM)), and hemostatic silicate nanodisks, LAPONITE®, as minimally invasive injectable hemostatic agents. Our T-STH is a physiologically stable hydrogel that can be easily injected through a syringe and needle and exhibits rapid mechanical recovery. Additionally, it demonstrates temperature-dependent blood coagulation owing to the phase transition of p(NIPAM). It decreases *in vitro* blood clotting times over 50% at physiological temperatures compared to room temperature. Furthermore, it significantly prevents blood loss in an *ex vivo* bleeding model at different blood flow rates (1 mL min^{-1} and 5 mL min^{-1}) by forming a wound plug. More importantly, our T-STH is comparable to a commercially available hemostat, Floseal, in terms of blood loss and blood clotting time in an *in vivo* rat liver bleeding model. Furthermore, once the hemorrhage is stabilized, our T-STH can be easily removed using a cold saline wash without any rebleeding or leaving any residues. Taken together, our T-STH can be used as a first aid hemostat to treat external hemorrhages in emergency situations.

Received 26th September 2022,
Accepted 7th December 2022

DOI: 10.1039/d2bm01559e

rsc.li/biomaterials-science

1. Introduction

Most battlefield injury-related mortalities occur in the pre-medical treatment facility environment before the injured soldier or victim can reach a hospital or a surgeon.[1] Of these, hemorrhage is responsible for most trauma-related mortality and is the leading cause of death on the battlefield.[1–4] Since 2008, QuikClot Combat Gauze® has been the gold standard for combat casualties by all US military branches. It is a gauze made of rayon and polyester blend loaded with kaolin, which helps control and stop bleeding by activating factor XII.[5–8] This product, however, cannot be used in noncompressible hemorrhages or internal bleeding.

Polymeric hydrogels have commonly been used for hemostasis and wound healing applications.[9–13] A variety of hemostats in the form of hydrogels,[14–16] sheets,[17,18] sponges,[19–21] and powders[22,23] have also been reported in the literature. Hydrogel-based hemostats, specifically have an added advantage due to their injectability and flowability which allows them to be used for fast and quick hemostasis from irregular-shaped wounds as well as intracavity injuries.[24] However, among them, very few hemostats meet the requirements for clinical translation. Therefore, there is a need for innovative multifactorial hemostats that can be used in an external wound *via* simple injection. An ideal hemostat for battlefield injuries and pre-medical treatment facility hemorrhage control should have the following characteristics:[25–28] (1) quick and adequate hemostasis in a wide range of injuries and wounds, (2) sustained hemostasis for several hours in situations of delayed evacuation, (3) easy removal without leaving any residues in the injury or wound, (4) ready to use and easy administration by a layperson with little to no training, (5) easy to manufacture and sterilize with low costs, (6) easily stored with prolonged stability even under extreme climate conditions, and (7) good biocompatibility with no adverse effects.

Shear-thinning hydrogels (STHs) can satisfy most of these requirements and have been developed using various materials.[29–33] STHs are engineered such that their viscosity reduces under high shear stress making these materials deform easily through syringes, needles, and catheters and rapidly retain their original form after removing the mechanical force. Our lab has previously explored gelatin and LAPONITE®-based STHs for hemorrhage control and endovas-

Terasaki Institute for Biomedical Innovation, Los Angeles, CA 90064, USA.
E-mail: mmecwan@terasaki.org, jjohn@terasaki.org, khademh@terasaki.org

† Electronic supplementary information (ESI) available. See DOI: https://doi.org/10.1039/d2bm01559e

cular embolization.[32,34] LAPONITE® (also sometimes referred to as silicate nanoplatelets) are highly charged nano-disks and have been shown to induce blood coagulation by interacting with platelets and concentrating clotting factors onto its surface.[32,34,35]

Thermoresponsive polymers, such as poly(*N*-isopropylacrylamide) or p(NIPAM), above their lower critical solution temperature (LCST), transit from a soluble hydrophilic state to an insoluble hydrophobic state which makes them useful for drug delivery applications. Furthermore, the polymer backbone can be modified with different polymers to tune the physical, mechanical, and drug release profile from these "smart" materials.[36,37] Several research groups have also explored thermoresponsive STHs for use in drug delivery,[38,39] 3D printing,[40–42] as well as a range of other medical applications.[43–45]

The motivation for this research is to develop a short-term reversible hemostat, one that could prevent external bleeding and stabilize the patient in emergency situations but could also be easily removed without leaving any residue once the patient was transported to a medical treatment facility. Additionally, it should be mechanically stable under physiological conditions, accelerate local hemostasis, and can be easily removed once the patient has been stabilized. Here, we engineered an injectable hydrogel hemostat to function as a hemostatic plug at physiological conditions (Fig. 1A). We combine LAPONITE®'s ability to aid in coagulation and the thermoresponsive nature of p(NIPAM) to engineer an injectable thermoresponsive STH or T-STH hemostat to stop bleeding. We hypothesize that the thermoresponsive nature of our T-STHs plays a critical role in aiding blood coagulation. Once the hemorrhage has been stabilized, being thermoresponsive the hemostat can be easily washed away using a cold saline wash to remove any debris from the wound, such as bullets and shrapnel. To this end, we assess the effect of varying p(NIPAM) concentrations on the rheological properties and injectability of the T-STHs. We then evaluated the thermoresponsive nature of our T-STHs and their ability to function as a hemostat using *in vitro* clotting studies and an *ex vivo* bleeding model. Finally, we validated our T-STH as injectable hemostats for minimally invasive treatments of hemorrhages using a rat liver bleeding model.

2. Results and discussion

2.1. T-STHs are thermoresponsive, injectable, and non-cytotoxic

Shear-thinning injectable materials have a lot of potential for developing minimally invasive therapies. LAPONITE® in its

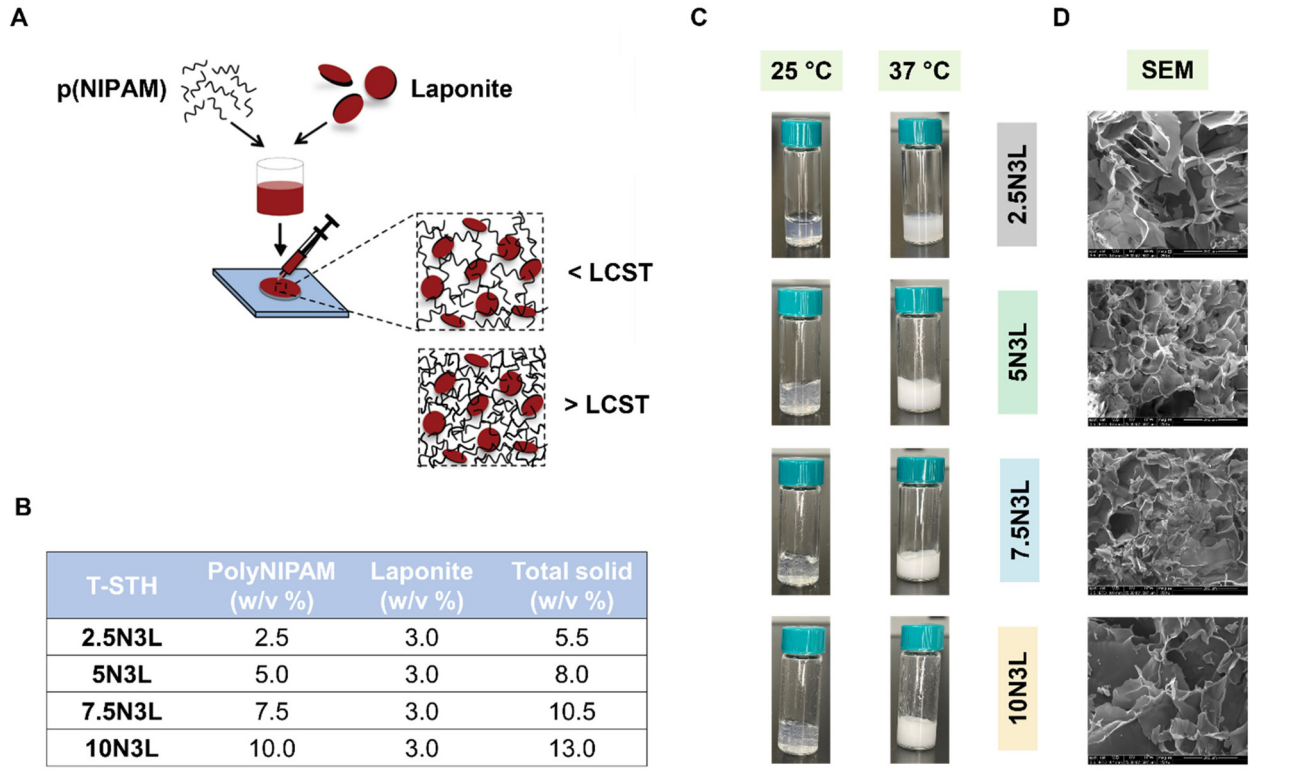

T-STH	PolyNIPAM (w/v %)	Laponite (w/v %)	Total solid (w/v %)
2.5N3L	2.5	3.0	5.5
5N3L	5.0	3.0	8.0
7.5N3L	7.5	3.0	10.5
10N3L	10.0	3.0	13.0

Fig. 1 (A) Schematic showing the preparation of our p(NIPAM) and LAPONITE®-based T-STH as an injectable hemostat for hemorrhage control. (B) Table summarizing the compositions of our p(NIPAM) and LAPONITE® T-STH formulations used in this study. (C) Representative images of our p(NIPAM) and LAPONITE®-based T-STH at 25 °C and at 37 °C. (D) Representative SEM images of our p(NIPAM) and LAPONITE®-based T-STH. The scale bar is 200 μm.

hydrated state exhibits shear-thinning properties.[46,47] Our lab, specifically, has developed shear-thinning hydrogels from porcine gelatin and LAPONITE® as embolic agents and drug delivery systems for the treatment hepatocellular carcinoma.[32,34,48,49] Inspired by our previous research, in this study, we engineered thermoresponsive hydrogels composed of p(NIPAM) and LAPONITE®. We wanted to take advantage of the thermoresponsive nature of p(NIPAM) to develop a reversible hemostat that would harden and form a wound plug at body temperature but could also be easily removed with a cold saline wash. Stock solution of p(NIPAM) and LAPONITE® were homogenized *via* vigorous agitation using a speed mixer to prevent clumping of the LAPONITE® during gelation. According to our previous research on gelatin-LAPONITE®-based STHs, LAPONITE® concentration of 3% w/w resulted in stable T-STHs that were effective in clotting blood for endovascular embolization.[32,34] For the fabrication of T-STH formulations, the LAPONITE® concentration was kept constant at 3 w/v%, while the p(NIPAM) concentration was varied from 2.5 w/v% to 10 w/v% (Fig. 1B).

The resulting T-STHs had a clear appearance at room temperature. Increasing p(NIPAM) concentration resulted in hydrogels that were more gelatinous in appearance. At 37 °C, the clear appearance changes to an opaque and white hydrogel (Fig. 1C). This is a result of the phase transition of p(NIPAM) from a hydrophilic state below its LCST to a hydrophobic state above its LCST. A video of the phase transition as the T-STH is being injected from a syringe at room temperature into water at 37 °C can be found in (ESI Video 1†). In addition, we also observed the microstructure of T-STH using SEM after freeze-drying (Fig. 1D). It appears that increasing p(NIPAM) concentration within the T-STH results in hydrogels with lower porosity. However, it should be noted that the actual porosity and pore sizes of the T-STH were not measured in this study and will need to be further investigated.

We investigated the rheological properties of our T-STHs using a rotational rheometer at both room temperature (25 °C) and body temperature (37 °C). Our T-STH formulations showed a slightly broader linear viscoelastic range (LVER) at 25 °C as compared to 37 °C, and the strain required to break the hydrogel network structure was greater than 10% at both temperatures. It should be noted that increasing the p(NIPAM) concentration in the T-STHs resulted in stronger gels at 25 °C (Fig. 2A). However, at 37 °C, a larger p(NIPAM) concentration resulted in slightly weaker gels (Fig. 2C). We hypothesize that at temperatures above the LCST, p(NIPAM) becomes more hydrophobic and interacts with its own polymer chains rather than the highly charged LAPONITE®, resulting in weaker gels. We also investigated the frequency-dependent rheology acquired in the LVER. For all samples, the G' exceeds the G'' values at both temperatures, indicating the formation of hydrogels. At 25 °C, the G' value of our T-STHs decreases with p(NIPAM) concentration, whereas, at 37 °C, the opposite trend is observed, indicating that p(NIPAM) contributes to the mechanical strength of our T-STHs (Fig. 2B and D). This is advantageous, as a higher G' at physiological temperatures would result in a harder gel that could function as a wound plug and prevent bleeding from a hemorrhaging wound.

To further explore the thermoresponsive behavior of our T-STHs, we investigated the temperature-dependent changes in G' and G'' values of our T-STH formulation, either through a slow temperature ramp from 15 °C to 45 °C or a sudden temperature change from 25 °C to 37 °C (Fig. 2E and F). The slow temperature ramp was carried out to observe the transition temperature of the T-STHs, while the sudden temperature change was performed to recapitulate the instance in which our T-STH would be applied to a bleeding patient (37 °C) from room temperature (25 °C). The data reveals that the G' values are always higher than the G'' values, which indicates that the T-STH is always in a hydrogel state. However, during the slow temperature ramp, we observe that the G' and G'' values start to increase around 31–32 °C which is comparable to the LCST of p(NIPAM) (~32 °C). This indicates that p(NIPAM) and LAPONITE® are held together by weak electrostatic interactions in our T-STHs. Furthermore, our results indicate that in response to a sudden temperature change from 25 °C to 37 °C, increasing p(NIPAM) concentration results in an increase as well as a faster change in G' and G'' values of our T-STHs.

Next, we studied the shear-thinning properties of our T-STH formulations at 25 °C (Fig. 3A and B) and 37 °C (Fig. 3D and E). For both temperatures, it was observed that p(NIPAM) concentration did not significantly affect the viscosity of T-STH, except in the cases of 2.5N3L and 10N3L ($p < 0.01$). However, a change in temperature from 25 °C to 37 °C resulted in significantly more viscous STHs for each formulation (ESI Fig. 1†). We also applied several cycles of a high strain (100% oscillatory strain) to break the network structure of the T-STH formulations, followed by low strain (1% oscillatory strain) to monitor the recovery of the storage modulus (G') of our T-STH at both room temperature and body temperature (Fig. 3C and F). At 25 °C, we observed that strain had minimal effect on the G' values of our T-STH. However, at 37 °C, the effect of strain was more pronounced. It should be noted, that at both temperatures, each of our T-STH formulations possesses excellent thixotropic recovery properties.

To assess the ease of injectability of our T-STH, we replicated the injection process using a mechanical tester. We measured the force required to inject our T-STH from 3 mL syringes either with or without a 23 G blunt needle (Fig. 4A). These experiments were only performed at room temperature. The force required to inject our T-STH from a 3 mL syringe (without a needle) ranged between 1–2 N, with no significant differences between the T-STH formulations. However, with a 23 G blunt needle, the applied force increased with increasing p(NIPAM) concentration and ranged from ~3.6 N for 2.5N3L to ~10.6 N for 10N3L (Fig. 4B). It was observed that in all cases, the applied force increased linearly until it plateaued at the injection force (Fig. 4C and D). These injection forces are easily achieved manually and do not require additional equipment for the application, allowing these T-STHs to be easily

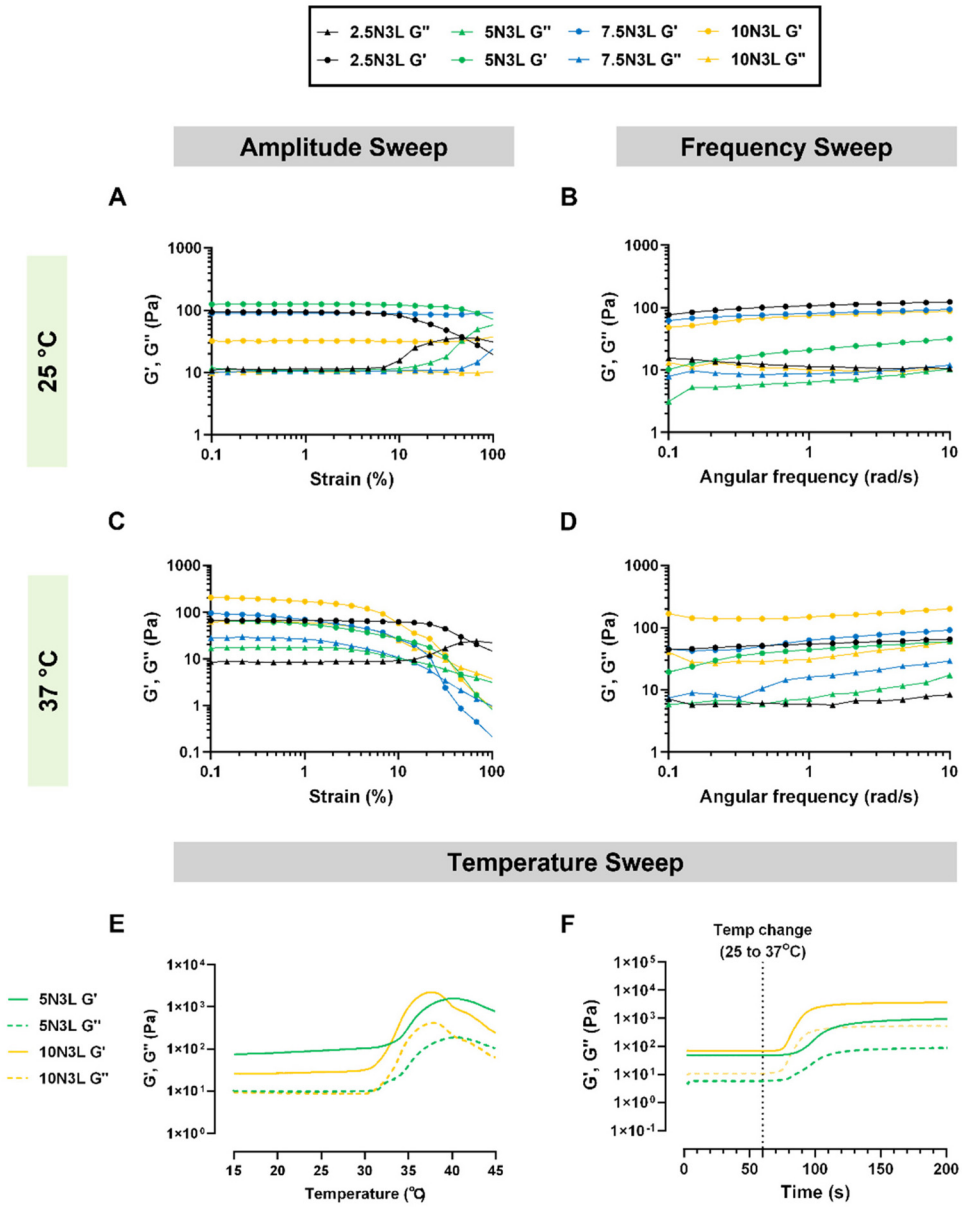

Fig. 2 Representative (A) amplitude sweep, and (B) frequency sweep of our p(NIPAM) and LAPONITE®-based T-STH at 25 °C. Representative (C) amplitude sweep, and (D) frequency sweep of our T-STH at 37 °C. The amplitude sweep was used to determine the linear viscoelastic range (LVER). The frequency sweeps were performed at 1% strain in the LVER of the T-STHs. Temperature-dependent change in G' and G'' values of our p(NIPAM) and LAPONITE®-based T-STHs (E) as the temperature slowly ramps up from 15 °C to 45 °C, and (F) as the temperature is suddenly changed from 25 °C to 37 °C.

implemented in emergency medical situations for application on external hemorrhaging wounds.

The short-term degradation of our T-STHs was investigated over 48 h under physiological conditions. We observed a slow degradation rate in PBS with approximately only 15% of mass loss (ESI Fig. 2A†). However, in human plasma, we noticed a faster degradation in the first 10 h (~35%) and little to no mass loss for the remainder of the experiment (ESI Fig. 2B†). It should be noted that there was no significant difference in the mass loss between all four T-STH formulations, suggesting that p(NIPAM) concentration does not affect the degradation of our T-STH. We speculate that the observed mass loss results from our T-STH being held together by weak physical and electrostatic interactions between p(NIPAM) and LAPONITE®. Since our T-STH hemostats are meant to be used for short-term use until the victim reaches a medical treatment facility (<24 h), the observed T-STH degradation is a non-issue.

We also demonstrated that our T-STHs were non-cytotoxic to NIH/3T3 fibroblasts over five days as determined by both

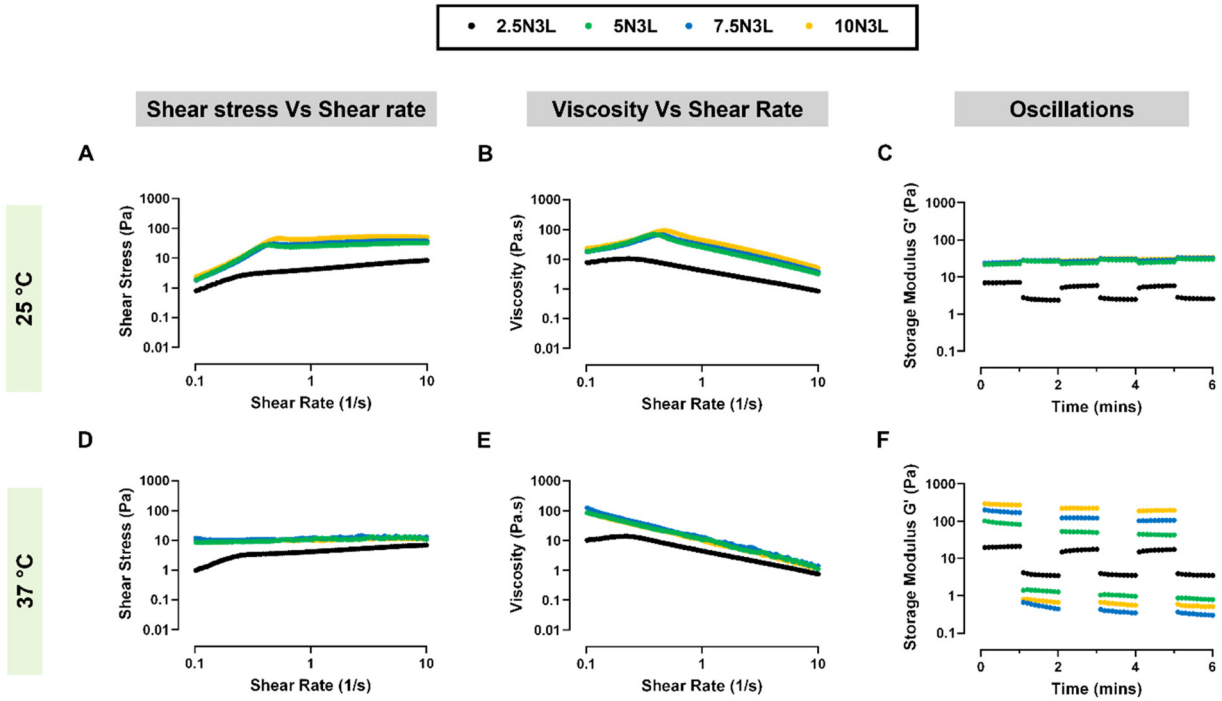

Fig. 3 Rheological properties of p(NIPAM) and LAPONITE®-based T-STH. Representative (A) shear stress *vs.* shear rate curves, (B) viscosity *vs.* shear rate curves, and (C) storage moduli (*G'*) after repeated applications of high strain (100% oscillatory strain) of our T-STH over time at 25 °C. Representative (D) shear stress *vs.* shear rate curves, (E) viscosity *vs.* shear rate curves, and (F) storage moduli (*G'*) after repeated applications of high strain (100% oscillatory strain) of our T-STH over time at 37 °C. Our T-STHs show a thermoresponsive change in rheological properties.

PrestoBlue™ cell viability and LIVE/DEAD assays (Fig. 5A and B). Furthermore, a 2-way ANOVA analysis of the normalized absorbance values determined no significant differences between the treatment groups or days. Moreover, hemolysis assays of diluted whole blood in contact with our T-STHs were performed to assess the hemocompatibility of our formulations. Fig. 5C shows that no significant differences between STB formulations which were comparable to previously reported values for other engineered hemostats.[34,50]

2.2. T-STHs promote temperature-dependent coagulation *in vitro*

Based on the initial characterization of our T-STH, which included rheological characterization, ease of injectability, and cytotoxicity testing, we decided to focus specifically on 5N3L and 10N3L for our blood coagulation experiments. The hemostatic ability of 5N3L and 10N3L was evaluated by monitoring the clotting time of whole blood in contact with our T-STH (Fig. 6A). The citrated whole blood (CWB) procured for these experiments coagulated in 11–12 min under physiological conditions (37 °C) after activation with $CaCl_2$. Under the same conditions, we observed similar clotting times for 5 wt% p(NIPAM). Increasing the p(NIPAM) concentration lowered the clotting time to 8–9 min, indicating that p(NIPAM) concentration affects clotting time. It has been previously hypothesized that negatively charged LAPONITE® interacts with platelets and other clotting factors in whole blood, which aids in coagulation.[32,34] Thus, incorporating LAPONITE® into our T-STH formulations further reduced clotting time to ~5.6 min for 10N3L and was comparable to 3 wt% LAPONITE® controls, which is over a 50% reduction in clotting time (Fig. 6B).

Interestingly, as seen in Fig. 6A, the clotting times for 5N3L and 10N3L at room temperature were comparable to activated CWB. We observed slight color change early on, which may be attributed to LAPONITE®; however, coagulation only occurred around 12 min. We speculate that below the LCST of p(NIPAM) (~32 °C), the polymer is in its soluble hydrophilic state and does not allow the blood to interact with LAPONITE®. However, above 32 °C, as the p(NIPAM) changes to an insoluble hydrophobic form, it entraps the blood within the polymer matrix and allows the LAPONITE® to interact with the blood better. This elucidates that the thermoresponsive behavior of our hemostats aid in the coagulation of blood. Moreover, we also measured the thrombus weights as a function of time for both 5N3L and 10N3L and observed a characteristic S-shaped curve with a clot starting to form around 3 min and plateaued out around 6–7 min (Fig. 6C), which correlated well with the clotting time data.

It is well known that platelets play an important role in the coagulation cascade. For a material to be hemostatic in nature it needs to exhibit strong platelet adhesion, activation and aggregation to the material surface. To demonstrate the hemostatic nature of T-STH hemostats, we performed a platelet

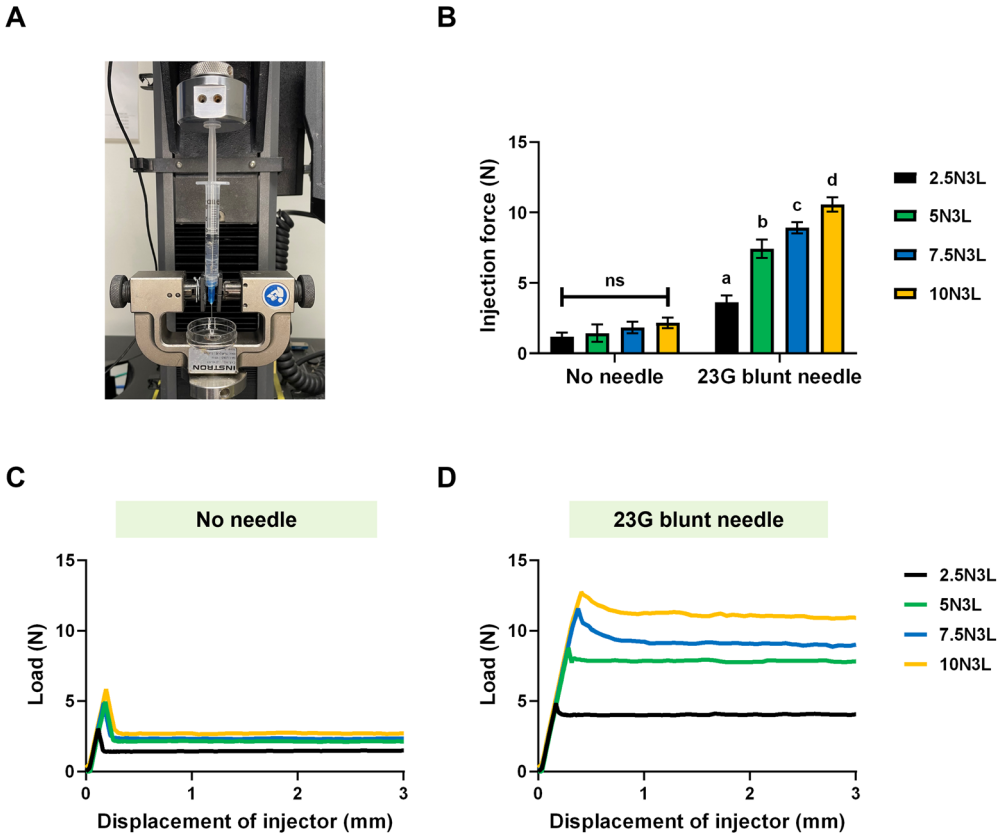

Fig. 4 Injectability of our p(NIPAM) and LAPONITE®-based T-STH. (A) Injection force measurement setup using an Instron mechanical tester. (B) Injection force of our T-STH through 3 mL syringes with no needle (no significant differences between T-STH formulations), and a 23 G blunt needle (*post hoc* Tukey's analysis determined significant differences between all pairwise comparisons $p < 0.01$ as indicated by different letters). Representative injection force curves required to inject our T-STH *via* a 3 mL syringe either with (C) no needle, and (D) a 23 G blunt needle. The average value of the plateau is used to quantify the injection force.

adhesion assay. After an hour of incubation of T-STH hemostats with PRP, we observed large number of platelets adhered and aggregated to the surface of both 5N3L and 10N3L surfaces (ESI Fig. 3†). This is not surprising, since it has been previously reported that the highly negative charge of LAPONITE® leads to platelet adhesion and activation, and eventually triggers the coagulation cascade.[32,51]

2.3. T-STH prevents blood loss at different blood flow rates in an *ex vivo* bleeding model

Following the *in vitro* blood clotting studies, for the remainder studies, we decided to focus on 10N3L to evaluate the efficacy of T-STH using an *ex vivo* bleeding model. Human blood vessel diameters range from 8 μm in capillaries to 25 mm for the aorta, with the blood flow rate in arteries and veins ranging from 3–26 mL min^{-1} and 1.2–4.8 mL min^{-1}, respectively. For our *ex vivo* studies, a syringe pump was used to flow human blood through medical-grade Tygon® tubing with an inner diameter of ~2.4 mm at either 1 mL min^{-1} or 5 mL min^{-1} (Fig. 7A). An "injury" was created by puncturing the tubing carrying blood with a 1.5 mm biopsy punch, and the amount of blood loss from the injury site was weighed after 5 min. For the untreated control, at the 1 mL min^{-1} blood flow rate, we observed approximately 1300 mg of blood loss. Not surprisingly, when the flow rate was increased to 5 mL min^{-1}, we observed four times increase in blood loss (~5200 mg).

In comparison, when treated with 1 mL of 10N3L, we observed a significant decrease in blood loss from the "injury" site for both 1 mL min^{-1} ($p < 0.05$) and 5 mL min^{-1} ($p < 0.01$) flow rates (Fig. 7B and C). At first, T-STH creates a physical barrier at the "injury" site, which prevents blood loss. Over time, in response to a change in temperature, witnessed by a change in appearance from clear to white (Fig. 7B), 10N3L forms a plug that prevents further blood loss at the "injury" site and prevents the tube from "bleeding out". It should be noted that a portable heater was used to maintain the ambient temperature around 37 °C at the "injury" site. As a result, the phase changes observed in 10N3L during the *ex vivo* study may not correctly replicate the body temperature. Despite this shortcoming, we were able to show that T-STH can effectively prevent blood loss from an "injury". Our *ex vivo* results, combined with *in vitro*

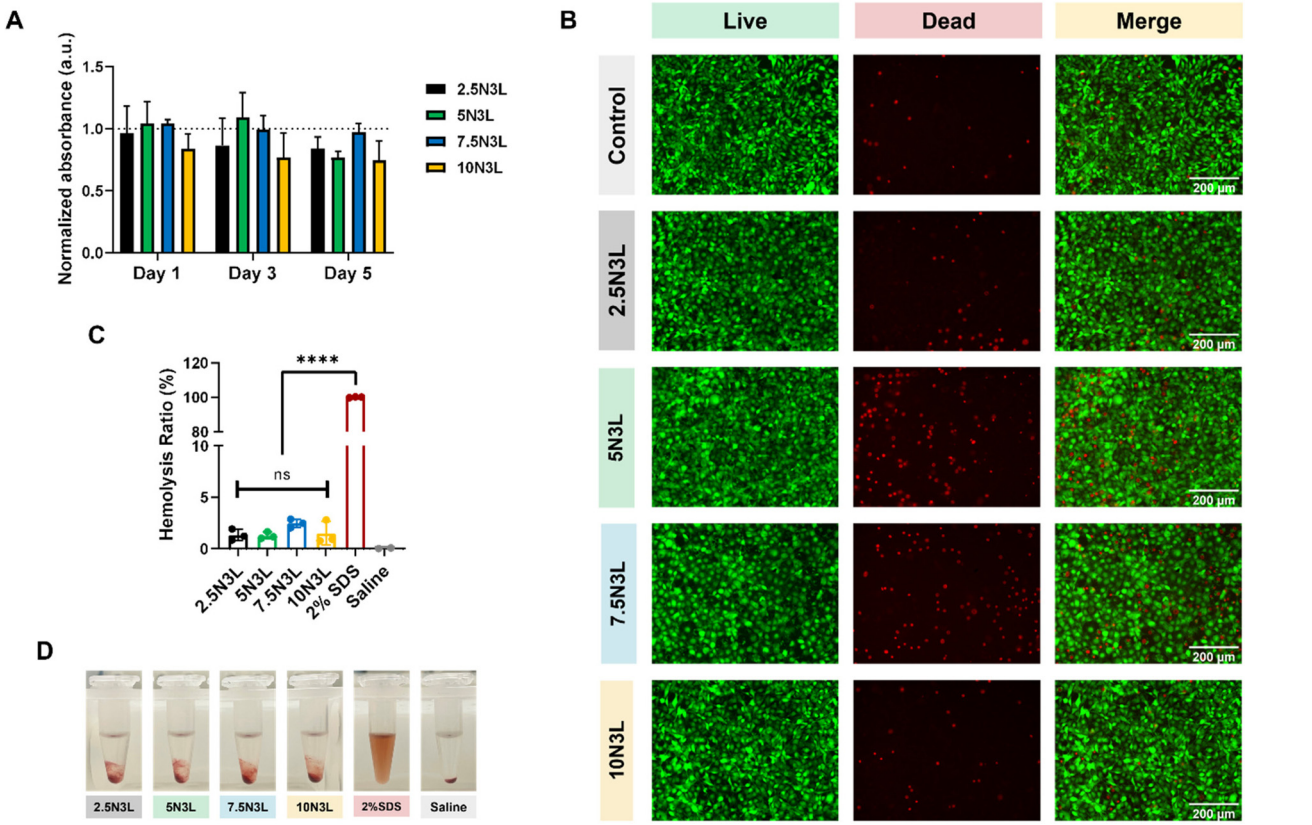

Fig. 5 *In vitro* cytocompatibility of our p(NIPAM) and LAPONITE®-based T-STH. (A) Quantitative analysis of NIH/3T3 mouse fibroblast cytotoxicity assay over five days using PrestoBlue™ cell viability reagent. Two-way ANOVA determined no significant difference between T-STH composition nor any significant difference between days. (B) Representative LIVE/DEAD images of NIH/3T3 mouse fibroblasts on day 5 of the cytotoxicity study. (C) Hemocompatibility analysis of red blood cell hemolysis in contact with our T-STH compared to 2% SDS (positive control) and saline (negative control). Two-way ANOVA analysis revealed no statistical differences between T-STHs. (D) Representative digital images of the hemocompatibility analysis of our T-STH compared to 2% SDS and saline.

blood coagulation results, show that T-STHs are effective hemostats for bleeding wounds and can prevent blood loss from bleeding veins and small arteries.

2.4. T-STH compares to commercially available hemostats in an *in vivo* liver bleeding model

An *in vivo* rat liver bleeding model was used to validate the hemostatic performance of our newly developed p(NIPAM) and LAPONITE®-based T-STH. We compared 10N3L against a commercially available hemostat, Floseal, an injectable hemostat matrix composed of gelatin and human thrombin. A schematic of the overall *in vivo* liver bleeding study can be found in Fig. 8A. Upon injury of the liver, blood loss and clotting times were used as determinants of effective hemostasis.

Representative images of the exposed liver (Fig. 8B) and amount of blood loss after treatment with or without hemostats can be found in Fig. 8C–E. The blood loss in the sham control, Floseal, and 10N3L treatment groups were 1121 ± 620 s, 1398 ± 848 s, and 372 ± 554 s respectively (Fig. 8F). The clotting time in the sham control group averaged 345 ± 75 s in the absence of hemostatic material treatment. However, the Floseal (35 ± 5 s) and 10N3L group (58 ± 21 s) stopped bleeding quickly (Fig. 8G). Blood clotting times for the treatment groups decreased significantly compared to sham controls, and it is worth noting that there were no significant differences between 10N3L and Floseal (p = 0.709). Therefore, treatment with 10N3L in the liver bleeding model resulted in lesser blood loss and comparable coagulation to Floseal, indicating that 10N3L contains functional components which could effectively improve hemorrhage control capability comparable to the speedy coagulation observed in Floseal which is attributed to thrombin. More importantly, these results demonstrate that T-STH achieved the 'standard of care' level for a commercially available hemostat in an *in vivo* bleeding model. Furthermore, the ease of applicability and removal of hemostats was investigated by observing untreated wounds, treated wounds, and wounds after the materials were removed using a cold saline wash. Compared to Floseal, there were no 10N3L residues on the wounds after the saline wash (ESI Fig. 4†). This is because as the temperature lowers below the LCST of p(NIPAM), 10N3L becomes more hydrophilic or hydrated and can be easily removed using a simple washing process (ESI Video 2†).

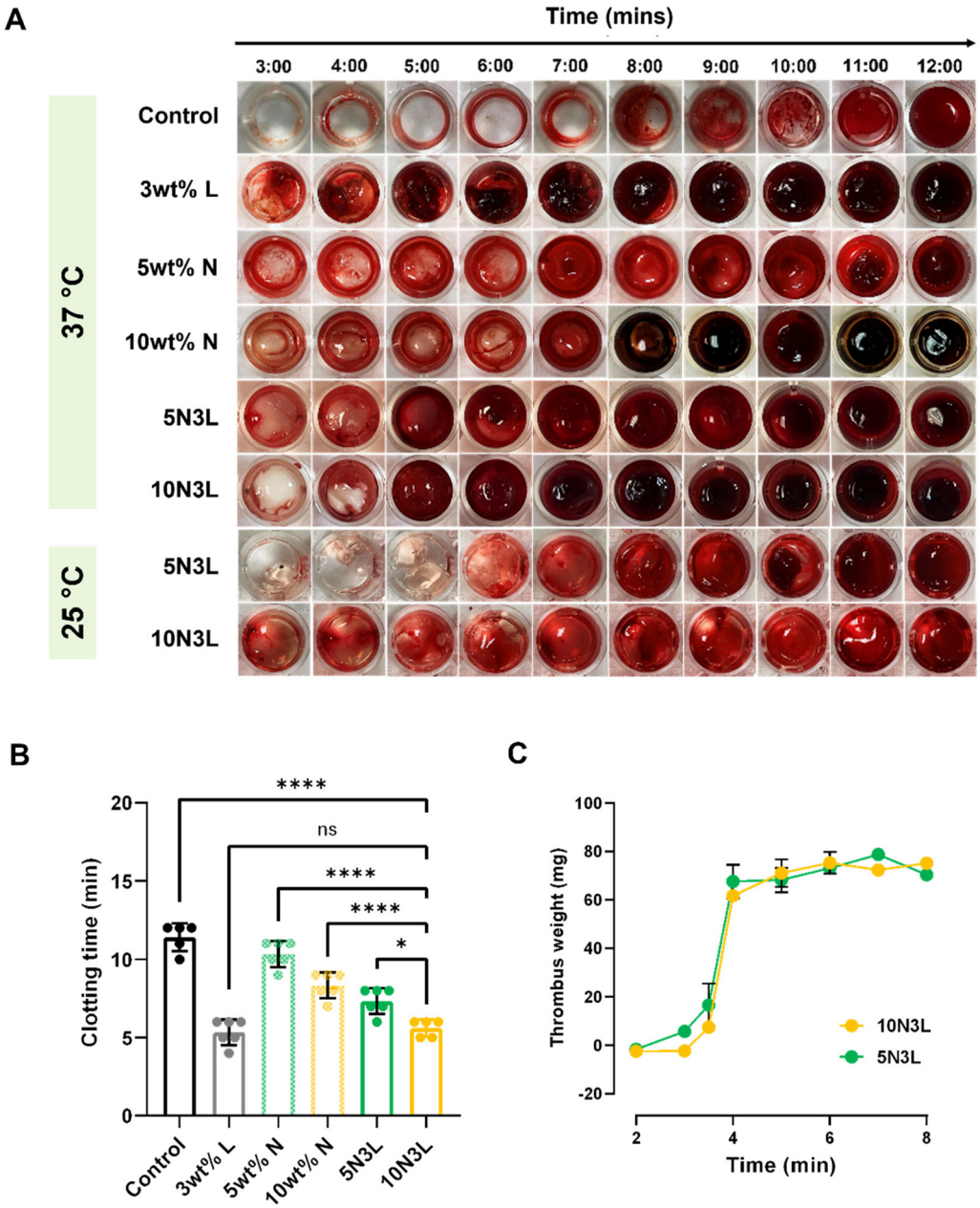

Fig. 6 *In vitro* evaluation of p(NIPAM) and LAPONITE®-based T-STHs as hemostats. (A) 48-Well plate assay of blood clotting in contact with control (polystyrene substrate), LAPONITE® control (3 w/v%), p(NIPAM) control (5 w/v% and 10 w/v%), and our T-STH (5N3L and 10N3L). T-STHs show temperature-dependent blood coagulation. (B) Quantitative clotting times as determined by the 48-well plate assay. One-way ANOVA followed by Tukey's *post hoc* analysis was performed; * $p < 0.05$; **** $p < 0.0001$. (C) Time series of clot formation by measuring the thrombus weight of T-STHs, 5N3L and 10N3L.

As previously discussed, hemorrhage control in the pre-medical treatment facility is critical for the survival of a patient, which drives the development of hemostatic materials for the battlefield and emergency first aid. Ideal hemostatic agents are biocompatible, non-cytotoxic, and beneficial for wound closure. Additionally, they are inexpensive and simple to use for a wide range of injuries. Floseal contains human thrombin, which helps convert fibrinogen to fibrin, and upon injection forms a crosslinked hemostatic plug to prevent bleeding. In comparison to Floseal, T-STH demonstrated promising results without the use of clotting factors. T-STHs enables indirect hemostasis *via* phase transition of p(NIPAM) to create a stable hemostatic wound plug at physiological temperatures and prevents blood loss from bleeding wounds independent of the normal coagulation mechanism. Additionally, LAPONITE® interacts with platelets to form the soft platelet plug, which eventually turns into a strong fibrin clot. Synergistically, the phase transition of p(NIPAM) and the platelet interaction and

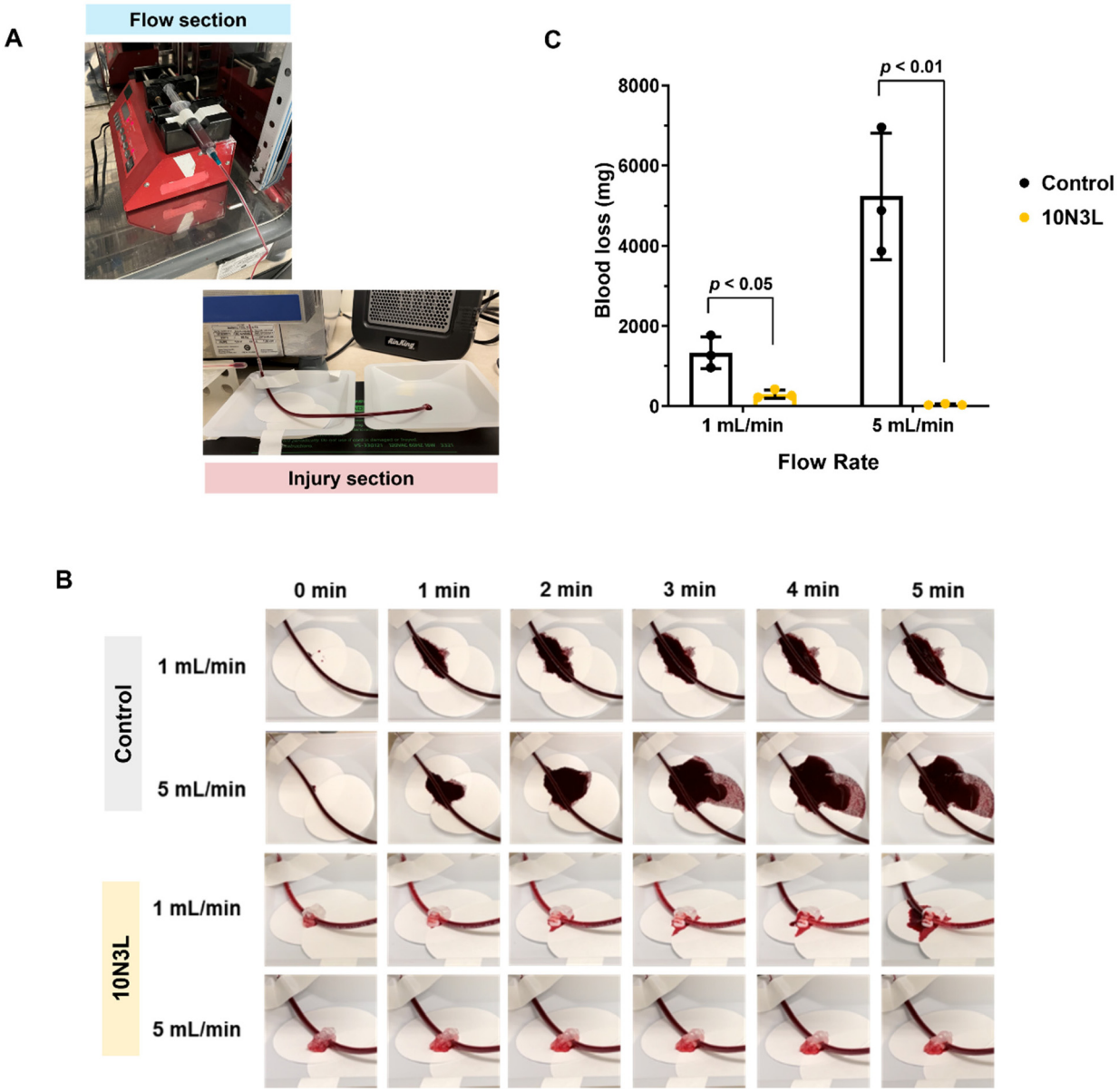

Fig. 7 *Ex vivo* bleeding model to test the efficacy of p(NIPAM) and LAPONITE®-based T-STHs as a hemostat. (A) Experimental setup of the *ex vivo* bleeding model with the "flow" section housed within a 37 °C incubator, and the "injury" section placed outside the incubator on a heating pad set at 37 °C. (B) Representative images of blood loss from an "injury" created by a 1.5 mm biopsy punch. 10N3L can create a plug at the "injury" site and prevent blood loss. (C) Quantitative blood loss (mg) from the "injury" after 5 min. Unpaired *t*-test was performed to determine statistical differences.

activation by LAPONITE® helps to form the wound plug and staunch hemorrhage from a bleeding wound.

Moreover, as compared to existing hydrogel-based hemostats and commercially available hemostats like Floseal, p(NIPAM) and LAPONITE® based T-STHs are reversible. Once the hemorrhage has been stabilized and the patient is safely transported to a hospital, T-STHs can be easily removed from the wound using a cold saline wash and not leave any residues behind. Recently, Liang *et al.* have developed adhesive hydrogel sealants that can be easily removed post-wound healing *via* dissolution.[52] Similarly, due to the thermoresponsive nature of our T-STH hemostats they can also be removed on-demand after achieving hemostasis. In emergency and battlefield settings, when T-STH is applied to a bleeding wound it will quickly undergo a phase transition to form a wound plug and prevent bleeding. Once the bleeding has stopped and the patient has been safely transported to a medical treatment facility, the T-STH hemostat can be washed away with cold saline without leaving any residue, and the clinician can perform appropriate surgery and treatment for the patient. This ability of easy application and removal of our T-STH provides first responders in emergency situations and

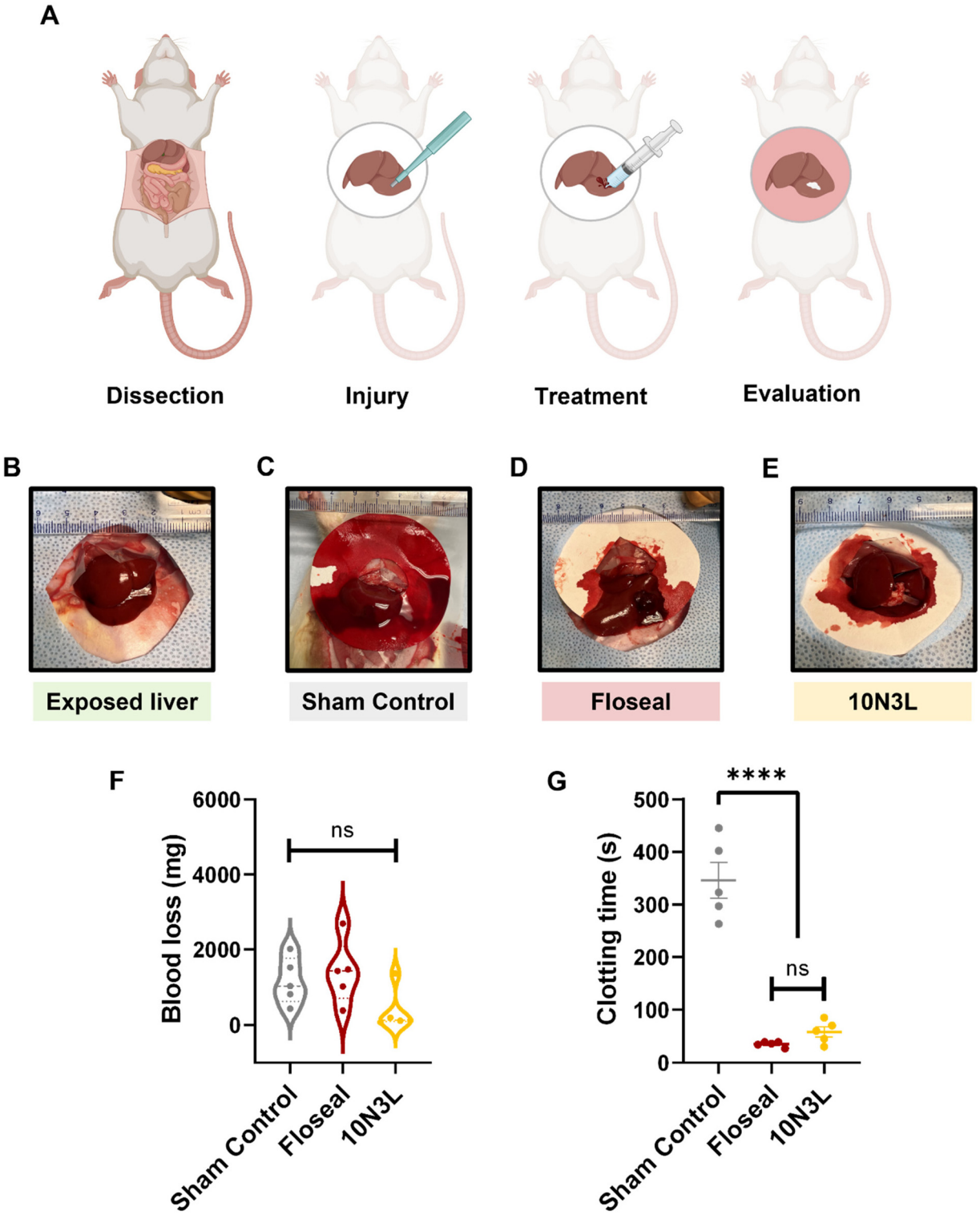

Fig. 8 *In vivo* rat liver bleeding model to validate p(NIPAM) and LAPONITE®-based T-STH as a hemostat. (A) Schematic of the *in vivo* bleeding model prepared using BioRender. The rat was dissected, and the liver was exposed (B) and placed on a Whatman filter paper. A biopsy punch (4 mm) was used to create and injury in the lower right lobe, and the wound was treated with three groups (n = 5): sham control (negative control), Floseal (commercial positive control), and 10N3L. Representative images of the bleeding liver after treatment with either (C) sham control, (D) Floseal, and (E) 10N3L. The (F) clotting time, and (G) blood loss from the wound after treating with the hemostatic materials. One-way ANOVA followed by a Tukey's *post hoc* analysis was performed to determine statistical differences between groups.

clinicians in hospital settings with an easy, yet effective minimally invasive tool for the treatment of external hemorrhages.

3. Conclusions

p(NIPAM) and LAPONITE®-based T-STHs formed injectable biomaterials that could be easily administered *via* a syringe, had higher G' values at physiological temperatures, were hemo- and cytocompatible, and promoted temperature-dependent *in vitro* coagulation. Of all T-STH compositions, 10N3L exhibited improved coagulation *in vitro*, significantly reduced blood loss in an *ex vivo* model from two different blood flow rates (1 and 5 mL min^{-1}), and was comparable to a commercially available hemostat, Floseal, in an *in vivo* rat bleeding model in terms of blood loss and clotting time. Moreover, T-STHs are mechanically stable under physiological conditions, accelerate local hemostasis without any clotting factors, and can be easily removed using a cold saline wash without leaving any residues. Due to these unique features, we believe T-STHs would function well in battlefield and emergency situations as an injectable hemostat first aid to treat external hemorrhages. Future studies will investigate the ability of T-STHs to be used for the delivery of other clotting factors for faster coagulation and antibiotics to prevent infections associated with injuries. Moreover, the delivery of regenerative signaling molecules for wound healing will also be investigated. Furthermore, with the intent to translate this technology into a viable product we will also explore the ability of T-STHs to be used as a sprayable hemostat for use in other types of wounds, such as blast injuries as well as lacerations and abrasion wounds.

4. Experimental section

4.1. Materials

For the preparation of T-STHs, p(NIPAM) (MW 40 000 Da) was purchased from Sigma Aldrich (Cat# 535311), and silicate nanoplatelets or LAPONITE®® XLG was purchased from BYK Additives Ltd. Citrated human whole blood was purchased from ZenBio (SER-WB). The blood type was O+ for the hemocompatibility studies and belonged to a 24-year-old African American male with a 35.7 BMI. For the *ex vivo* studies, the blood type was also O+ and belonged to a 53-year-old Hispanic male with a 25.68 BMI. In addition, calcium chloride ($CaCl_2$) solution (0.1 M) and 0.9% saline solution was purchased from Spectrum Chemical Manufacturing Corp (C-092) and Teknova (S5815), respectively.

4.2. Preparation of thermoresponsive STH (T-STH) formulations and SEM imaging

Stock solutions of p(NIPAM) (20 w/v%) and LAPONITE® (12 w/v%) were prepared in Milli-Q water (4 °C). Four different T-STH formulations (Fig. 1B) were prepared by vortexing appropriate ratios of the p(NIPAM) stock, LAPONITE® stock, and Milli-Q water. The T-STH formulations had a general formula xNyL, where x = 2.5, 5, 7.5 and 10 w/v% of p(NIPAM), and y = 3 w/v% of LAPONITE®. The vortexing was done 3 times, at 3000 rpm for 5 min using a SpeedMixer™ (DAC 150.1 FVZ), and the T-STHs were stored overnight at 4 °C before use.

The temperature-dependent phase transition of the T-STH was observed by taking digital images of the samples at room temperature and at 37 °C. The morphology of dried T-STH with various compositions was characterized by scanning electron microscopy (SEM) (FEI Quanta 200, Hillsboro, OR). All samples for SEM imaging were kept at −80 °C for 24 h, freeze-dried for 48 h, and mounted onto a metallic stub using double-sided conductive carbon tape. Samples were then sputter-coated in an Ar atmosphere with an Au–Pd target at a peak current of 15 μA for 5 min and subsequently imaged using an accelerating voltage of 15–25 kV.

4.3. Rheological analysis and injectability of T-STH

T-STH shear rate, frequency sweeps, and recoverability were analyzed according to previously reported protocols with minor modifications.[32,34,38] An Anton Paar MCR 302 rheometer was used for mechanical testing, and the data was recorded *via* Anton Paar Rheocompass software. Shear stress, viscosity, and storage moduli were measured with a 25 mm diameter parallel plate geometry with a rough surface, and a gap height of 500 μm was used. Mineral oil was added around the plate to prevent water evaporation from the T-STH once the sample was loaded. All T-STHs were equilibrated for 5 min before testing, followed by a 2 min steady shear at 10 s^{-1}. Steady shear rate sweeps investigated the shear-thinning properties of the samples at 25 and 37 °C, and the viscosities of the materials were measured as a function of shear rate. Step-rate time-sweep was performed to investigate the thixotropic recovery properties of the samples between low shear strain (1%) and high shear strain (100%) at 25 and 37 °C. Oscillation amplitude sweep and frequency sweeps were applied to measure the storage modulus (G') and loss modulus (G'') of the samples at 37 °C. Temperature sweeps from 15 to 45 °C at a heating rate of 1 °C min^{-1} were carried out to measure gelation temperature, whereas time sweeps at 37 °C were performed to investigate the gelation kinetics.

The injectability of T-STHs was analyzed using an Instron (Model 5542). Briefly, the T-STH was added to a 3 mL syringe and centrifuged at 2000 rpm for 5 min to pack the T-STH within each syringe. The T-STHs were then injected through the syringe either with no needle or a 23 G blunt needle (BD biosciences) using standard Luer-lock fittings. The syringe plunger was depressed using an upper compressive platen. The housing of the syringe or needle was fitted into a lower tensile grip to prevent movement during the experiment. An injection rate of 33.33 mL min^{-1} was used for these tests, and the force on the plunger was measured with a 100 N load cell and recorded using Bluehill version 3 software. The plateau's average injection force (N) was obtained by quintuple measure-

ments of three identical compositions of each T-STH formulation.

4.4. Degradation of T-STH

T-STH degradation was performed either in PBS or human plasma. First, human plasma was separated from citrated human whole blood by centrifugation at 3000 rpm for 15 min (Beckman Coulter Allegra™ 6R centrifuge) and stored at −80 °C until use. Next, 0.2 mL of each T-STH formulation was injected into 1.5 mL Eppendorf tubes, centrifuged to flatten, and weighed (~175–200 mg). Then, 1 mL of pre-warmed PBS or human plasma was added to each sample and placed in a benchtop orbital shaker at 37 °C with constant shaking at 100 rpm (Barnstead Lab-Line MaxQ 4000). After incubation for 1, 3, 6, 10, 24, 30, and 48 h, the PBS or human plasma was removed, and the remaining T-STH was weighed. Each sample was replaced with either fresh PBS or human plasma and returned to the incubator. The relative weight percentage of each T-STH was defined as $W\% = (W_r/W_0) \times 100$, where W_r is the weight of the remaining T-STH at various time points, and W_0 is the weight of T-STH at the initial state. T-STH degradation studies in both PBS and human plasma were performed in triplicates, and mass remaining (%) is reported as mean ± standard deviation of the replicates.

4.5. Cytotoxicity and hemocompatibility assessment studies

NIH/3T3 cells (ATCC, CRL 1658) were cultured in Dulbecco's modified Eagle's medium (Gibco, 1165092) and supplemented with 10% heat inactivated fetal bovine serum (Gibco™), 50 μg mL^{-1} streptomycin, and 50 U mL^{-1} penicillin in 5% CO_2 at 37 °C. Cells were seeded in a 24-well plate (1×10^4 cells per well) and grown for 24 h with 1 mL of complete growth media. Next, 0.2 mL of T-STH was injected into transwell inserts (Costar, 3396) and sterilized *via* UV sterilization for 30 min. The eluates from the T-STH samples in the transwell inserts were then transferred to the 24-well plate with NIH 3T3 cells, and fresh complete growth media was added (1 mL) to the T-STH samples in the transwell inserts and changed daily throughout the experiment. Cytotoxicity was assessed at days 1, 3, and 5 using PrestoBlue™ cell viability reagent (A13261, ThermoFisher) following the manufacturer's protocol. Transwell inserts without any T-STH were used as controls. All data were normalized to the controls and reported as mean ± standard error means of all replicates.

Hemolysis testing was performed according to previously published protocols.[34,50] Citrated human whole blood was diluted 50× with 0.9% (w/v) saline solution. First, 0.1 mL of T-STH were injected into 1.5 mL Eppendorf tubes and briefly centrifuged to evenly flatten each sample. Next, 1 mL of diluted blood was added to each tube and incubated at 37 °C under agitation (100 rpm). After 2 h, the Eppendorf tubes were centrifuged at 14 000 rpm for 10 min, the supernatants were transferred into wells of a 96-well plate, and the absorbance of the supernatants was read at 542 nm. Saline and 2% SDS were used as negative and positive controls, respectively. Percent hemolysis was defined as $H\% = [(A_{sample} - A_{neg})/A_{pos}] \times 100$, where A_{sample} is the absorbance at 542 nm of the T-STH-containing supernatant, A_{neg} is the absorbance of the saline-diluted blood, and A_{pos} is the absorbance of the DI water-diluted blood. These hemolysis studies were performed in triplicates, and the hemolysis ratio (%) is reported as mean ± standard deviation of all replicates.

4.6. *In vitro* blood clotting studies

Clotting times were measured according to previously reported protocols with minor variations.[32,34] A volume of 630 μL of citrated whole blood was pipetted into a 1.5 mL Eppendorf tube, and a volume of 70 μL of 0.1 M $CaCl_2$ was then added, followed by vortexing for 10 s, to reactivate the blood. Immediately, 0.2 mL of the blood was transferred to 48-well plates. At every minute between 3 and 12 min, each well was washed with 0.9% saline solution to halt clotting. The liquid was immediately aspirated, and the samples were washed repeatedly until the wash solution was clear, indicating complete removal of blood components. For the T-STH samples, 0.2 mL of T-STH was injected into wells of a 48-well plate and centrifuged at 2000 rpm for 10 min to evenly flatten each sample. The final clotting time was determined when a uniform clot was formed, with no change in clot size in subsequent wells. These clotting time studies were performed at room temperature (~25 °C) and 37 °C in triplicates for each time point.

Thrombus weights were determined according to previously published protocols with minor variations.[32] Briefly, 0.1 mL of either 5N3L or 10N3L were injected into 1.5 mL Eppendorf tubes, followed by a short centrifuge cycle to flatten out each sample, and the tubes containing the T-STHs were weighed. Next, citrated human whole blood was reactivated with 0.1 M $CaCl_2$ at a 9 : 1 ratio and vortexed for 10 s. Immediately, 0.1 mL of the blood was pipetted into the tubes containing the T-STH, and the tubes were transferred to an Eppendorf ThermoMixer® C maintained at 37 °C under constant agitation at 300 rpm. At each time point, clotting was stopped by adding 1 mL of 0.9% saline solution, followed by saline washes, until the wash solution was clear. Finally, the Eppendorf tubes with the newly formed clots were reweighed to determine the thrombus weights produced in the tubes. These studies were performed in triplicates for each time point, and the weight of the thrombus (mg) is reported as the mean ± standard deviation of all replicates.

4.7. *In vitro* platelet adhesion studies

Platelet adhesion to our T-STH were performed using previously published protocols.[53] To obtain platelet-rich plasma (PRP), fresh citrated whole blood was centrifuged at 95*g* for 15 min at 8 °C. The transparent layer or PRP was transferred to another vial and the RBC layer was discarded. 200 μL of PRP was dispensed onto the dried T-STH samples and incubated at 37 °C for 1 h. After incubation, the samples were gently rinsed three times with PBS, and the adherent platelets were fixed with 4 v/v% paraformaldehyde (in PBS) overnight at 4 °C. After fixation, the samples were rinsed in PBS (three times) and

serial dehydrated with 10%, 25%, 50%, 75%, 90%, and 100% ethanol for 10 min each. The dehydrated samples were mounted onto a metallic stub using double-sided conductive carbon tape. Samples were then sputter-coated in an Ar atmosphere with an Au–Pd target at a peak current of 15 μA for 5 min and subsequently imaged with a ZEISS Supra 40VP SEM using an accelerating voltage of 12 kV. The platelet adhesion results were interpreted qualitatively by observing the SEM images.

4.8. *Ex vivo* bleeding model

The *ex vivo* bleeding model setup had two sections. The "flow" section comprised a syringe pump (Braintree Scientific, Model BS8000) housed in an incubator to maintain the blood temperature at 37 °C. Medical grade tubing was used as artificial blood vessels (Tygon® tubing ND-100-65; inner diameter 3/32″ and outer diameter 5/32″) to flow blood from the "flow" section to the "injury" section, which was outside the incubator but placed on a heating pad (VIVOSUN reptile heat mat and digital thermostat combo) set to 37 °C and a portable heater (AIR KING non-oscillating portable electric heater) was used to maintain the ambient temperature at 37 °C. An image of the *ex vivo* bleeding model setup can be found in Fig. 7A.

Briefly, 0.1 M $CaCl_2$ solution was mixed with citrated whole blood at a 1 : 9 ratio, and vortexed for 10 s. The activated blood was gently transferred to a syringe and was secured in the syringe pump. A 23 G needle with Tygon® tubing was then attached to the syringe. To mimic various blood flow rates in the body, these experiments were performed at two different flow rates: 1 mL min^{-1} and 5 mL min^{-1}. Once the blood started flowing at the end of the tube, an "injury" was created approximately 10″ from the tubing end using a 1.5 mm biopsy punch to puncture the tube. The "injury" was either left untreated (control) or 1 mL of 10N3L was applied to the injury site. At every minute, from t = 0 min to 5 min, a digital image was taken, and the amount of blood loss (mg) was measured by weighing the Whatman filter paper at the end of the experiment (5 min). The *ex vivo* studies were performed in triplicates, and the amount of blood loss (mg) is reported as the mean ± standard deviation of all replicates.

4.9. *In vivo* rat liver bleeding model

15 male rats were purchased from Charles River and housed in an animal facility (Lundquist Institute, Torrance, CA) at a controlled temperature of 23 ± 1 °C, and humidity of 55 ± 5%, in a 14 h light/10 h dark cycle for one week before the animal procedure. All the animal experiments were performed with the approval of the Institutional Animal Ethics Committee of the Lundquist Institute (IACUC number: 32705-01), where the study was executed following the guidelines of the Committee for Control and Supervision of Experimental Animals, USA. On the day of surgery, all animals were randomly divided into 3 groups (n = 5): sham control, commercially available Floseal hemostatic matrix (Baxter), and our T-STH composed of 10N3L. All the equipment were sterilized and dried in a sterile environment before the procedure. The animals were anesthetized using isoflurane inhalation (1–4%), and under anesthesia, the surgery site was shaved and sterilized with betadine, and an incision was made horizontally to expose the liver. The left middle lobe of the liver was lifted upward, placed on a Whatman weighing paper, and a standardized liver wound (4 mm) was created with a disposable surgical biopsy punch at the base of the lobe. After wound bleeding, the speed and initial amount of bleeding were qualified for subsequent hemostatic experiments. The animals were then treated with different hemostatic agents on the liver wound to stop the bleeding. For example, the sham control group, underwent active bleeding without any hemostatic treatment. In the second and third group, the bleeding liver was treated with commercially available Floseal (0.1 mL) and 10N3L (0.1 mL), respectively, on the bleeding site. The clotting time after applying the experimental material (control and hemostats) and the amount of blood loss was measured by weighing the Whatman paper.

4.10. Graphing and statistical analysis

GraphPad Prism 9 software was used for graphing and plotting data for this research, as well as for performing statistical analysis. When appropriate a one-way ANOVA analysis, followed by a Tukey's *post hoc* analysis, was used to determine statistical differences between treatment groups. For the cytotoxicity studies, a two-way ANOVA analysis was performed to determine statistical differences between treatment groups and between days. For the *ex vivo* bleeding studies, an unpaired Student's t-test was used to observe any statistical difference in blood loss between the control and 10N3L treatment group. In all cases, α was set to 0.05.

Conflicts of interest

There are no conflicts to declare.

Acknowledgements

The authors would like to acknowledge funding from the National Institute of Health (5R01HL137193) and the Terasaki Institute of Biomedical Innovation.

References

1 B. J. Eastridge, R. L. Mabry, P. Seguin, J. Cantrell, T. Tops, P. Uribe, O. Mallett, T. Zubko, L. Oetjen-Gerdes, T. E. Rasmussen, F. K. Butler, R. S. Kotwal, J. B. Holcomb, C. Wade, H. Champion, M. Lawnick, L. Moores and L. H. Blackbourne, Death on the battlefield (2001–2011): implications for the future of combat casualty care, *J. Trauma Acute Care Surg.*, 2012, **73**(6 Suppl 5), S431–S437.

2 D. S. Kauvar, R. Lefering and C. E. Wade, Impact of Hemorrhage on Trauma Outcome: An Overview of Epidemiology, Clinical Presentations, and Therapeutic Considerations, *J. Trauma Acute Care Surg.*, 2006, **60**(6), S3–S11.

3 J. B. Holcomb, N. R. McMullin, L. Pearse, J. Caruso, C. E. Wade, L. Oetjen-Gerdes, H. R. Champion, M. Lawnick, W. Farr, S. Rodriguez and F. K. Butler, Causes of death in U.S. Special Operations Forces in the global war on terrorism: 2001–2004, *Ann. Surg.*, 2007, **245**(6), 986–991.
4 E. L. Mazuchowski, R. S. Kotwal, J. C. Janak, J. T. Howard, H. T. Harcke, H. R. Montgomery, F. K. Butler, J. B. Holcomb, B. J. Eastridge, J. M. Gurney and S. A. Shackelford, Mortality review of US Special Operations Command battle-injured fatalities, *J. Trauma Acute Care Surg.*, 2020, **88**(5), 686–695.
5 Y. Ran, E. Hadad, S. Daher, O. Ganor, J. Kohn, Y. Yegorov, C. Bartal, N. Ash and G. Hirschhorn, QuikClot Combat Gauze Use for Hemorrhage Control in Military Trauma: January 2009 Israel Defense Force Experience in the Gaza Strip—A Preliminary Report of 14 Cases, *Prehosp. Disaster Med.*, 2010, **25**(6), 584–588.
6 B. Gegel, J. Burgert, J. Gasko, C. Campbell, M. Martens, J. Keck, H. Reynolds, M. Loughren and D. Johnson, The Effects of QuikClot Combat Gauze and Movement on Hemorrhage Control in a Porcine Model, *Mil. Med.*, 2012, **177**(12), 1543–1547.
7 G. Basadonna, QuikClot Combat Gauze for Hemorrhage Control, *Prehosp. Disaster Med.*, 2012, **27**(2), 217–217.
8 M. W. Cripps, C. C. Cornelius, P. A. Nakonezny, N. Vazquez, J. C. Wey and P. E. Gales, In vitro effects of a kaolin-coated hemostatic dressing on anticoagulated blood, *J. Trauma Acute Care Surg.*, 2018, **85**(3), 485–490.
9 M. Mecwan, J. Li, N. Falcone, M. Ermis, E. Torres, R. Morales, A. Hassani, R. Haghniaz, K. Mandal, S. Sharma, S. Maity, F. Zehtabi, B. Zamanian, R. Herculano, M. Akbari, J. V. John and A. Khademhosseini, Recent advances in biopolymer-based hemostatic materials, *Regener. Biomater.*, 2022, **9**, rbac063.
10 Z. Pan, H. Ye and D. Wu, Recent advances on polymeric hydrogels as wound dressings, *APL Bioeng.*, 2021, **5**(1), 011504.
11 B. Guo, R. Dong, Y. Liang and M. Li, Haemostatic materials for wound healing applications, *Nat. Rev. Chem.*, 2021, **5**(11), 773–791.
12 R. Dong, H. Zhang and B. Guo, Emerging hemostatic materials for non-compressible hemorrhage control, *Natl. Sci. Rev.*, 2022, **9**(11), nwac162.
13 S. Pourshahrestani, E. Zeimaran, N. A. Kadri, N. Mutlu and A. R. Boccaccini, Polymeric Hydrogel Systems as Emerging Biomaterial Platforms to Enable Hemostasis and Wound Healing, *Adv. Healthcare Mater.*, 2020, **9**(20), 2000905.
14 M. N. Sundaram, S. Amirthalingam, U. Mony, P. K. Varma and R. Jayakumar, Injectable chitosan-nano bioglass composite hemostatic hydrogel for effective bleeding control, *Int. J. Biol. Macromol.*, 2019, **129**, 936–943.
15 M. Sakoda, M. Kaneko, S. Ohta, P. Qi, S. Ichimura, Y. Yatomi and T. Ito, Injectable Hemostat Composed of a Polyphosphate-Conjugated Hyaluronan Hydrogel, *Biomacromolecules*, 2018, **19**(8), 3280–3290.
16 S. Bian, L. Hao, X. Qiu, J. Wu, H. Chang, G.-M. Kuang, S. Zhang, X. Hu, Y. Dai, Z. Zhou, F. Huang, C. Liu, X. Zou, W. Liu, W. W. Lu, H. Pan and X. Zhao, An Injectable Rapid-Adhesion and Anti-Swelling Adhesive Hydrogel for Hemostasis and Wound Sealing, *Adv. Funct. Mater.*, 2022, **32**(46), 2207741.
17 S. Ohta, T. Nishiyama, M. Sakoda, K. Machioka, M. Fuke, S. Ichimura, F. Inagaki, A. Shimizu, K. Hasegawa, N. Kokudo, M. Kaneko, Y. Yatomi and T. Ito, Development of carboxymethyl cellulose nonwoven sheet as a novel hemostatic agent, *J. Biosci. Bioeng.*, 2015, **119**(6), 718–723.
18 Y. Izumi, M. Gika, N. Shinya, S. Miyabashira, T. Imamura, C. Nozaki, M. Kawamura and K. Kobayashi, Hemostatic Efficacy of a Recombinant Thrombin-Coated Polyglycolic Acid Sheet Coupled With Liquid Fibrinogen, Evaluated in a Canine Model of Pulmonary Arterial Hemorrhage, *J. Trauma Acute Care Surg.*, 2007, **63**(4), 783–787.
19 X. Huang, Y. Sun, J. Nie, W. Lu, L. Yang, Z. Zhang, H. Yin, Z. Wang and Q. Hu, Using absorbable chitosan hemostatic sponges as a promising surgical dressing, *Int. J. Biol. Macromol.*, 2015, **75**, 322–329.
20 Y. He, J. Wang, Y. Si, X. Wang, H. Deng, Z. Sheng, Y. Li, J. Liu and J. Zhao, A novel gene recombinant collagen hemostatic sponge with excellent biocompatibility and hemostatic effect, *Int. J. Biol. Macromol.*, 2021, **178**, 296–305.
21 G. Lan, B. Lu, T. Wang, L. Wang, J. Chen, K. Yu, J. Liu, F. Dai and D. Wu, Chitosan/gelatin composite sponge is an absorbable surgical hemostatic agent, *Colloids Surf., B*, 2015, **136**, 1026–1034.
22 B. S. Kheirabadi, J. W. Edens, I. B. Terrazas, J. S. Estep, H. G. Klemcke, M. A. Dubick and J. B. Holcomb, Comparison of New Hemostatic Granules/Powders With Currently Deployed Hemostatic Products in a Lethal Model of Extremity Arterial Hemorrhage in Swine, *J. Trauma Acute Care Surg.*, 2009, **66**(2), 316–328.
23 J. Li, X. Wu, Y. Wu, Z. Tang, X. Sun, M. Pan, Y. Chen, J. Li, R. Xiao, Z. Wang and H. Liu, Porous chitosan microspheres for application as quick in vitro and in vivo hemostat, *Mater. Sci. Eng., C*, 2017, **77**, 411–419.
24 J. Cheng, J. Liu, M. Li, Z. Liu, X. Wang, L. Zhang and Z. Wang, Hydrogel-Based Biomaterials Engineered from Natural-Derived Polysaccharides and Proteins for Hemostasis and Wound Healing, *Front. Bioeng. Biotechnol.*, 2021, **9**, 780187.
25 H. T. Peng, Hemostatic agents for prehospital hemorrhage control: a narrative review, *Mil. Med. Res.*, 2020, **7**(1), 13.
26 T. Peng, Biomaterials for hemorrhage control, *Trends Biomater. Artif. Organs*, 2010, **24**(1), 27–68.
27 M. C. Neuffer, J. McDivitt, D. Rose, K. King, C. C. Cloonan and J. S. Vayer, Hemostatic Dressings for the First Responder: A Review, *Mil. Med.*, 2004, **169**(9), 716–720.
28 A. E. Pusateri, A. V. Delgado, E. J. J. Dick, R. S. Martinez, J. B. Holcomb and K. L. Ryan, Application of a Granular Mineral-Based Hemostatic Agent (QuikClot) to Reduce Blood Loss After Grade V Liver Injury in Swine, *J. Trauma Acute Care Surg.*, 2004, **57**(3), 555–562.
29 C. Xue, H. Xie, J. Eichenbaum, Y. Chen, Y. Wang, F. W. van den Dolder, J. Lee, K. Lee, S. Zhang, W. Sun, A. Sheikhi,

S. Ahadian, N. Ashammakhi, M. R. Dokmeci, H. J. Kim and A. Khademhosseini, Synthesis of Injectable Shear-Thinning Biomaterials of Various Compositions of Gelatin and Synthetic Silicate Nanoplatelet, *Biotechnol. J.*, 2020, **15**(8), e1900456.

30 Y. Pang, J. Liu, Z. L. Moussa, J. E. Collins, S. McDonnell, A. M. Hayward, K. Jajoo, R. Langer and G. Traverso, Endoscopically Injectable Shear-Thinning Hydrogels Facilitating Polyp Removal, *Adv. Sci.*, 2019, **6**(19), 1901041.

31 S. Xia, Z. Ding, L. Luo, B. Chen, J. Schneider, J. Yang, C. G. Eberhart, W. J. Stark and Q. Xu, Shear-Thinning Viscous Materials for Subconjunctival Injection of Microparticles, *AAPS PharmSciTech*, 2020, **22**(1), 8.

32 A. K. Gaharwar, R. K. Avery, A. Assmann, A. Paul, G. H. McKinley, A. Khademhosseini and B. D. Olsen, Shear-Thinning Nanocomposite Hydrogels for the Treatment of Hemorrhage, *ACS Nano*, 2014, **8**(10), 9833–9842.

33 H. D. Lu, M. B. Charati, I. L. Kim and J. A. Burdick, Injectable shear-thinning hydrogels engineered with a self-assembling Dock-and-Lock mechanism, *Biomaterials*, 2012, **33**(7), 2145–2153.

34 R. K. Avery, H. Albadawi, M. Akbari, Y. S. Zhang, M. J. Duggan, D. V. Sahani, B. D. Olsen, A. Khademhosseini and R. Oklu, An injectable shear-thinning biomaterial for endovascular embolization, *Sci. Transl. Med.*, 2016, **8**(365), 365ra156–365ra156.

35 S. E. Baker, A. M. Sawvel, N. Zheng and G. D. Stucky, Controlling Bioprocesses with Inorganic Surfaces: Layered Clay Hemostatic Agents, *Chem. Mater.*, 2007, **19**(18), 4390–4392.

36 M. A. Haq, Y. Su and D. Wang, Mechanical properties of PNIPAM based hydrogels: A review, *Mater. Sci. Eng., C*, 2017, **70**, 842–855.

37 R. R. Kokardekar, V. K. Shah and H. R. Mody, PNIPAM Poly (N-isopropylacrylamide): A thermoresponsive "smart" polymer in novel drug delivery systems, *Internet J. Med. Update-EJOURNAL*, 2012, **7**(2), 59–62.

38 Z. Liu and P. Yao, Injectable thermo-responsive hydrogel composed of xanthan gum and methylcellulose double networks with shear-thinning property, *Carbohydr. Polym.*, 2015, **132**, 490–498.

39 N. A. Jalili, M. K. Jaiswal, C. W. Peak, L. M. Cross and A. K. Gaharwar, Injectable nanoengineered stimuli-responsive hydrogels for on-demand and localized therapeutic delivery, *Nanoscale*, 2017, **9**(40), 15379–15389.

40 S. H. Hsiao and S. H. Hsu, Synthesis and Characterization of Dual Stimuli-Sensitive Biodegradable Polyurethane Soft Hydrogels for 3D Cell-Laden Bioprinting, *ACS Appl. Mater. Interfaces*, 2018, **10**(35), 29273–29287.

41 A. Abbadessa, M. M. Blokzijl, V. H. Mouser, P. Marica, J. Malda, W. E. Hennink and T. Vermonden, A thermo-responsive and photo-polymerizable chondroitin sulfate-based hydrogel for 3D printing applications, *Carbohydr. Polym.*, 2016, **149**, 163–174.

42 L. Hahn, E. Karakaya, T. Zorn, B. Sochor, M. Maier, P. Stahlhut, S. Forster, K. Fischer, S. Seiffert, A. C. Pöppler, R. Detsch and R. Luxenhofer, An Inverse Thermogelling Bioink Based on an ABA-Type Poly(2-oxazoline) Amphiphile, *Biomacromolecules*, 2021, **22**(7), 3017–3027.

43 A. L. A. Binch, L. P. D. Ratcliffe, A. H. Milani, B. R. Saunders, S. P. Armes and J. A. Hoyland, Site-Directed Differentiation of Human Adipose-Derived Mesenchymal Stem Cells to Nucleus Pulposus Cells Using an Injectable Hydroxyl-Functional Diblock Copolymer Worm Gel, *Biomacromolecules*, 2021, **22**(2), 837–845.

44 M. J. Glassman, J. Chan and B. D. Olsen, Reinforcement of Shear Thinning Protein Hydrogels by Responsive Block Copolymer Self-Assembly, *Adv. Funct. Mater.*, 2013, **23**(9), 1182–1193.

45 L. Wu, H. Zhou, H. J. Sun, Y. Zhao, X. Yang, S. Z. Cheng and G. Yang, Thermoresponsive bacterial cellulose whisker/poly(NIPAM-co-BMA) nanogel complexes: synthesis, characterization, and biological evaluation, *Biomacromolecules*, 2013, **14**(4), 1078–1084.

46 H. Z. Cummins, Liquid, glass, gel: The phases of colloidal LAPONITE®, *J. Non-Cryst. Solids*, 2007, **353**(41–43), 3891–3905.

47 A. Sheikhi, S. Afewerki, R. Oklu, A. K. Gaharwar and A. Khademhosseini, Effect of ionic strength on shear-thinning nanoclay-polymer composite hydrogels, *Biomater. Sci.*, 2018, **6**(8), 2073–2083.

48 J. Lee, Y. Wang, C. Xue, Y. Chen, M. Qu, J. Thakor, X. Zhou, N. R. Barros, N. Falcone, P. Young, F. W. van den Dolder, K. Lee, Y. Zhu, H.-J. Cho, W. Sun, B. Zhao, S. Ahadian, V. Jucaud, M. R. Dokmeci, A. Khademhosseini and H.-J. Kim, pH-Responsive doxorubicin delivery using shear-thinning biomaterials for localized melanoma treatment, *Nanoscale*, 2022, **14**(2), 350–360.

49 Q. Wu, M. Qu, H.-J. Kim, X. Zhou, X. Jiang, Y. Chen, J. Zhu, L. Ren, T. Wolter, H. Kang, C. Xu, Z. Gu, W. Sun and A. Khademhosseini, A Shear-Thinning Biomaterial-Mediated Immune Checkpoint Blockade, *ACS Appl. Mater. Interfaces*, 2022, **14**(31), 35309–35318.

50 V. A. Kumar, N. L. Taylor, A. A. Jalan, L. K. Hwang, B. K. Wang and J. D. Hartgerink, A nanostructured synthetic collagen mimic for hemostasis, *Biomacromolecules*, 2014, **15**(4), 1484–1490.

51 G. Lokhande, J. K. Carrow, T. Thakur, J. R. Xavier, M. Parani, K. J. Bayless and A. K. Gaharwar, Nanoengineered injectable hydrogels for wound healing application, *Acta Biomater.*, 2018, **70**, 35–47.

52 Y. Liang, Z. Li, Y. Huang, R. Yu and B. Guo, Dual-Dynamic-Bond Cross-Linked Antibacterial Adhesive Hydrogel Sealants with On-Demand Removability for Post-Wound-Closure and Infected Wound Healing, *ACS Nano*, 2021, **15**(4), 7078–7093.

53 H. S. Nanda, A. H. Shah, G. Wicaksono, O. Pokholenko, F. Gao, I. Djordjevic and T. W. J. Steele, Nonthrombogenic Hydrogel Coatings with Carbene-Cross-Linking Bioadhesives, *Biomacromolecules*, 2018, **19**(5), 1425–1434.